atmosphere

MDPI

Article

Contribution of the Incinerator to the Inorganic Composition of the PM_{10} Collected in Turin

Eleonora Conca [1], Mery Malandrino [1,*], Agnese Giacomino [2], Paolo Inaudi [2], Sandro Buoso [1], Stefano Bande [3], Milena Sacco [3] and Ornella Abollino [2]

1 Department of Chemistry, University of Turin, Via P. Giuria 5, 10125 Turin, Italy; eleonora.conca@unito.it (E.C.); sandro.buoso@unito.it (S.B.)
2 Department of Drug Science and Technology, University of Turin, Via P. Giuria 9, 10125 Turin, Italy; agnese.giacomino@unito.it (A.G.); paolo.inaudi@unito.it (P.I.); ornella.abollino@unito.it (O.A.)
3 Piedmont Regional Agency for the Environmental Protection, Via Pio VII 9, 10135 Turin, Italy; stefano.bande@arpa.piemonte.it (S.B.); milena.sacco@arpa.piemonte.it (M.S.)
* Correspondence: mery.malandrino@unito.it; Tel.: +39-011-6705249

Received: 14 March 2020; Accepted: 15 April 2020; Published: 17 April 2020

Abstract: Modern incinerator plants are equipped with an efficient system for the removal of pollutants and, hence, the gas and particle emissions are generally extremely low. However, it is possible that malfunctions, together with specific meteorological conditions, temporarily cause significant emissions. In this study, the evolution of the inorganic composition of PM_{10} samples collected in the vicinity of the Turin incinerator before and after its commissioning was assessed. The purpose was to identify the PM sources present in the area, and to evaluate if the operation of the incinerator caused an increase of the concentration of some species. Significant differences were registered among the composition of samples collected in 2012 and 2014, as the latter year was characterized by higher concentrations of Al, As, Ba, Ca, K, Na, Ni, Pb, Sr, and Zn. Considering the position of the incinerator and of the monitoring station, it seems that this increment was not directly caused by the plant emissions. The most probable source of these elements is the highway vehicular traffic, which might have increased due to the travelling of trucks carrying wastes to the incinerator. However, a direct contribution deriving from the incinerator emissions cannot be excluded.

Keywords: incinerator, Turin (Italy); PM_{10}; inorganic composition; chemometric treatments

1. Introduction

The concentration and the composition of the atmospheric particulate matter (PM) in urban areas is nowadays widely monitored, due to the risks it poses to human health [1–6]. The health risks associated with PM arise from the possibility of deposition of particles in the human respiratory system; in particular, the depth that particles can reach strictly depends on the particle size [7,8]. Besides their size, the damages the particles can cause to the organism are strongly related to their chemical composition [9]. One of the main sources of urban atmospheric particulate matter is vehicular traffic [10–12], but other sources such as industries or waste treatment plants can sometimes represent important sources of PM [13].

In recent years, according to the European directives (e.g., 2008/98/CE), landfill waste disposal has been progressively abandoned in favor of procedures which allow the recovery of materials and energy [14–16]. Waste-to-energy incinerators are waste treatment plants able to convert municipal solid waste into energy, generating ash and gas as residues [16,17]. In this way, fossil fuel can be saved, and the waste volume can be remarkably reduced [13,18]. The modern plants are equipped with an efficient system for the removal of pollutants from the gaseous emissions. Therefore, according to the

stricter and stricter emission limits set by the local and European regulations, the gas and particle emissions are generally extremely low [14,18–20]. However, it is possible that malfunctions, together with specific meteorological conditions, cause the limits to be exceeded [13]. In the broader context of urban air quality monitoring, hence, it is extremely important to continuously monitor the incinerator emissions, in order to be sure that the pollutant removal systems are properly working and to be able to immediately stop the plant in the event of an exceedance of maximum allowable limits [18].

In the Turin metropolitan area, one single municipal solid waste incinerator plant is present. Its construction started on 8 February, 2010 and its commissioning started on 19 April, 2013. In 2014, approximately 403x10^6 kg of waste was burned, generating 294 GWh of electric energy [21]. The plant is composed of three twin lines, and the pollutant abatement systems include electrofilters (for the removal of PM), the injection of activated carbon and sodium bicarbonate (for the removal of acids, organic compounds, and metals), and selective catalytic reduction reactors (for the reduction of NOx) [17,21].

In this study, the evolution of the inorganic composition of PM_{10} collected in the vicinity of the Turin incinerator before and after its commissioning was assessed. The purpose was to identify the PM sources present in the area, and to evaluate if the operation of the incinerator caused an increase of the concentration of some species. A wide variety of elements, namely Al, As, Ba, Ca, Cd, Ce, Co, Cr, Cu, Fe, K, La, Mg, Mn, Mo, Na, Ni, Pb, Sb, Sr, Ti, V, and Zn, and the major ions, namely Ca^{2+}, Cl^-, K^+, Mg^{2+}, Na^+, NH_4^+, NO_3^-, and SO_4^{2-}, were analyzed.

2. Experiments

2.1. Apparatus and Reagents

The dissolution of samples was performed by means of a Milestone ETHOS One microwave laboratory unit. The determination of the elemental composition of samples was carried out using high-resolution inductively coupled plasma mass spectrometry (HR-ICP-MS) and inductively coupled plasma optical emission spectrometry (ICP-OES), according to the concentration levels; wavelength, mass resolution, and isotope selection were optimized for each element in order to minimize spectral interferences and maximize the sensitivity. Three certified reference materials (CRMs), namely BCR 176 ("city waste incineration fly ash"), NIST 1648a ("urban particulate matter"), and NIES 8 ("vehicle exhaust particulates"), were used for evaluating the procedural recovery and for identifying the best analytical parameters.

The determination of the water-soluble ion concentrations was carried out using ion chromatography (IC). For the determination of the cation concentration, a polymeric column functionalized with carboxylic and phosphonic groups (Dionex CS12A) was used, and 20 mM methanesulfonic acid was used as eluent. For the determination of the anion concentration, a polymeric column functionalized with ammonium groups (Dionex AS18) was used, and high purity water (HPW) was used as eluent. The analysis of cations and anions was simultaneously performed, as the autosampler automatically split the samples among the two columns. The model and features of each instrument are reported in Table S1. The detection limits (DL), corresponding to three times the standard deviation of the reagent blank, were experimentally determined. The optimized analytical parameters and the experimental DL are reported in Table S2.

For the digestion of samples, Sigma-Aldrich nitric acid (65%) and hydrogen peroxide (30%) were used. Water was purified in a Milli-Q system, resulting in HPW with a resistivity of 18.2 MΩ·cm. Intermediate standard solutions were prepared from concentrated (1000 mg/L) stock solutions (Sigma-Aldrich TraceCERT) and acidified.

2.2. Study Area and Sampling

The PM_{10} sampling was performed in Beinasco (Italy), in the monitoring station managed by the Piedmont Regional Environmental Protection Agency (ARPA Piemonte). The station was built in 2012

at 1.1 km southeast from the incinerator, specifically for its monitoring, i.e., in the residential area which, according to the local meteorological conditions, was expected to be the most strongly affected by the incinerator emissions. The maximum fallout area was identified by means of the CALPUFF integrated modeling system (Sigma Research Corporation, 1990), i.e., an integrated Lagrangian puff modeling system constituted by a diagnostic 3D meteorological model, an air quality dispersion model, and a postprocessing package. A map of the metropolitan area, showing the position of the incinerator and the monitoring station, is reported in Figure 1. The sampler was a TCR Tecora Charlie, with a Sentinel module for the automatic sequential sampling. The PM_{10} samples were collected on a daily basis on Millipore AQFA04700 hydrophilic quartz filters. The sampling flow was approximately 55 m^3/day.

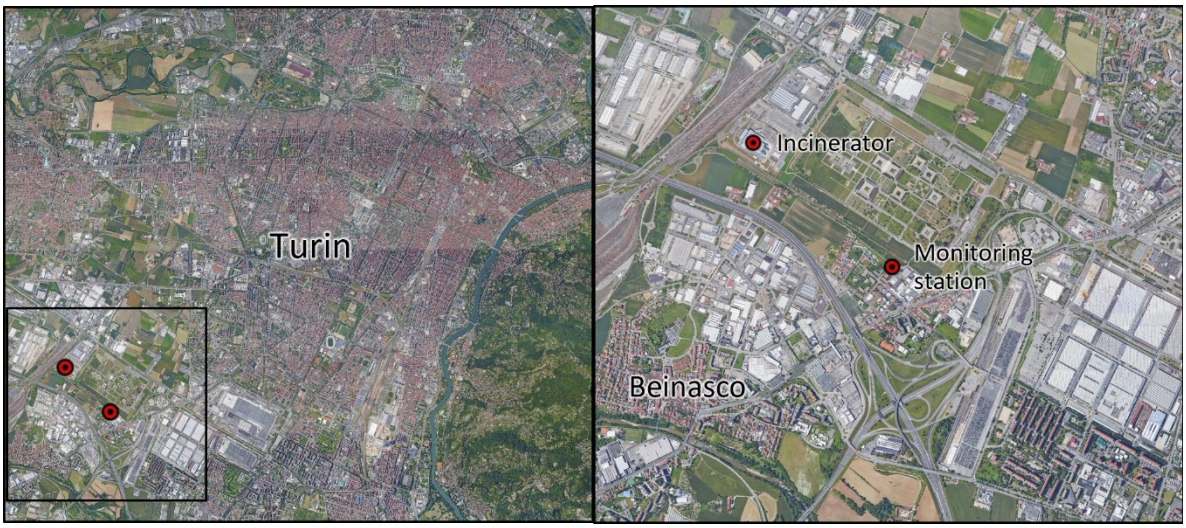

Figure 1. Google Earth maps showing the position of the incinerator and the monitoring station: (**a**) Turin metropolitan area; (**b**) zoom of the investigated site.

In order to evaluate the effect of the incinerator emissions on the inorganic composition of the PM_{10} collected in Beinasco, two sampling campaigns were performed: one before and one after the commissioning. In the first sampling campaign, 82 samples were collected from 4th October to 31st December 2012. In the second sampling campaign, 92 samples were collected from 1st October to 31st December 2014.

2.3. Choice of the Samples

In order to reduce the number of samples to analyze without losing information, the meteorological conditions of each sampling campaign were investigated and, with the aid of chemometrics, a statistical sample representative of each identified condition was chosen. Besides the proper meteorological information (i.e., average and maximum wind speed, average and maximum mixing height, and average temperature), the gravimetric PM_{10} and $PM_{2.5}$ mass concentrations and the NO and NO_2 atmospheric concentrations were used (Table S3).

In 2012, the monitoring station was still not fully functional, therefore the local meteorological data were calculated with the diagnostic meteorological MINERVE model (Aria Technologies, 2001). MINERVE [22], a mass-consistent model based on mass conservation and minimization of wind field divergence, was implemented by ARPA Piemonte [23] in order to reconstruct the 3D wind and temperature fields of the Beinasco area, starting from the meteorological information collected in the nearest ARPA monitoring stations and from the European Center For Medium Range Weather Forecast (ECMWF) background fields. The MINERVE implementation proved to have a good accuracy in the reconstruction of the wind field over all the areas described by the model at a resolution of 4 km [24–26]. This model is capable of simulating air pollutant emissions, transport, diffusion, and

chemical reactions, to estimate concentration fields for the main atmospheric pollutants on an hourly basis over the whole Piedmont territory.

On the other hand, the 2014 meteorological data were directly measured in the Beinasco monitoring station. The average and maximum mixing height values were calculated by means of SURFPRO software [27,28]. SUFRPRO computes the mixing-layer height starting from the output of MINERVE model, using the Maul et al. version [29] of Carson encroachment method for the diurnal mixing-layer height and the minimum value between the formulas of Nieuwstadt [30] and Venkatram [31] for the nocturnal mixing-layer height.

The missing values (less than 15% of the total $PM_{2.5}$ mass concentration) were calculated with the NIPALS algorithm, and the dataset was then autoscaled. Principal component analysis (PCA) and hierarchical cluster analysis (HCA) were performed and jointly used for the choice of the samples to analyze. A minimum of 55% of the samples constituting each cluster identified by HCA was chosen. A total of 50 samples collected in 2012 and 46 samples collected in 2014 were analyzed.

2.4. Sample Pretreatment and Analysis

In order to obtain the PM_{10} mass concentration, the filters were weighed before and after the sampling. Prior to each weighing, the samples were conditioned for 48 h at controlled temperature and humidity (T = 20 ± 1 °C; rh = 50% ± 5%). Each filter was then cut into two pieces with plastic scissors and tweezers: one half was dedicated to the elemental analysis and the other half to the water-soluble ion analysis.

According to the European guide for the measurement of potentially toxic elements in PM_{10} samples (UNI EN 14902:2015), the microwave-assisted dissolution of samples for the determination of the elemental composition was performed by means of a mixture composed by 3.5 mL HNO_3, 1.5 mL H_2O_2, and 3 mL HPW. One half of each filter and the digestion mixture were introduced into 100 mL tetrafluoro me tho xyl vessels and the temperature was ramped to 170 °C within 5 min, followed by a dwell time of 10 min, and then ramped to 200 °C within 5 min, followed by a dwell time of 20 min. After a sufficient cooling time, the vessels were opened and the solution was filtered with Whatman Grade 5 cellulose filters, previously cleaned with 20 mL HPW, and then diluted to 30 mL. The calibration standard solutions were prepared by the addition of the standards to a solution obtained by microwave-digesting the reagent mixture only (matrix-matching method). According to the European guide for the measurement of cations and anions in $PM_{2.5}$ samples (CEN/TR 16269:2011), the other half of each filter was posed in contact with 10 mL HPW in a polypropylene 15 mL container, and then subjected to 500 kW ultrasounds for 30 min. The solution was then filtered with Millipore Millex-HV hydrophilic polyvinylidene fluoride syringe filters (pore size: 0.45 µm). Sets of instrumental blank and calibration checks were run at frequent intervals during the analysis sequences. In Section 3, uncharged and charged symbols (e.g., Na and Na^+) refer to the total and water-soluble element concentrations, respectively.

2.5. Statistic Data Analysis

The experimental results were processed by chemometric treatments using XlStat 2017 software package, an add-on of Microsoft Excel. The non-parametric Mann–Whitney test (one-sided, significance level: 95%) was performed for verifying if the analyte concentrations or the anthropogenic portion of the analytes were significantly higher in 2014 than in 2012 samples. Moreover, principal component analysis (PCA) was performed. PCA is a powerful statistical technique that provides an orthogonal transformation of the original variables into new and uncorrelated variables, called principal components (PCs). The PCs represent a linear combination of the original variables, that ensures that most of the dataset variance is retained in the first few PCs. More information on the principles of these techniques can be found elsewhere [32–36]. The analytes whose concentrations were below the DL in more than 30% of samples were not included in the treatments [37]. Regarding the other

analytes, for performing PCA, values below the DL were considered as equal to it; the whole dataset was then autoscaled.

3. Results and Discussion

The inorganic composition of the analyzed samples collected in 2012 and 2014 are reported in Tables S4, S5 and S6, S7, respectively. As expected for urban PM_{10} samples, the major elements are Ca, Fe, K, Mg, and Na, and the major ions are Cl^-, NH_4^+, NO_3^-, and SO_4^{2-}. Figure 2 reports pie charts showing the average composition of the samples collected in the two sampling campaigns. The percentage of each analyte was calculated with respect to the gravimetric PM_{10} mass concentrations, therefore the undetermined portion of the PM_{10} ("Undet." in the charts), most likely constituted by silicates, elemental carbon, and organic components, is also reported. The analytes representing less than 1% of the PM_{10} are globally represented under the heading "Sum". The main difference among the average composition of 2012 and 2014 samples lies in the undetermined components, which decreased from 62% to 45%. Consequently, most of the other components (i.e., Ca, K, Mg, Na, NH_4^+, NO_3^-, and SO_4^{2-}) represent a higher portion of the samples. Exceptions are Fe, which remained stable on 2%, and Cl^-, which reduced from 2.1% to 0.6%.

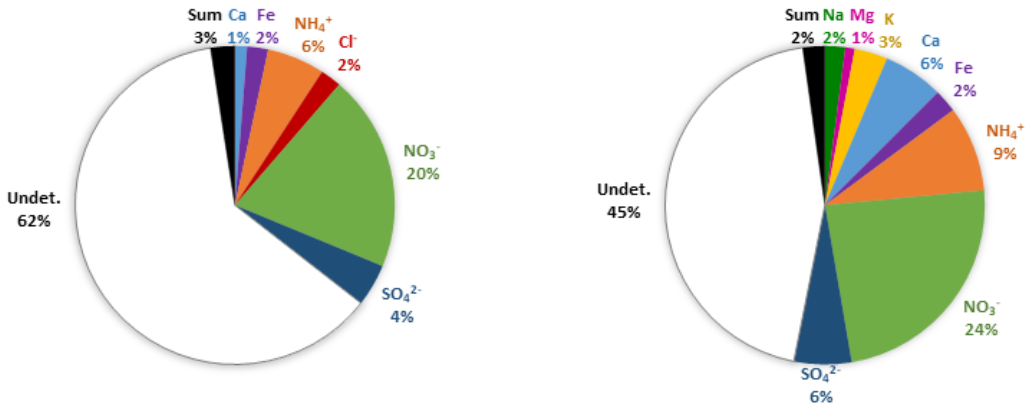

Figure 2. Average composition of the PM_{10} samples collected in (**a**) 2012; (**b**) 2014.

According to their molar concentrations, the analyzed water-soluble ions can be ordered as follows: $NH_4^+ > NO_3^- >> SO_4^{2-} > Cl^- \approx Ca^{2+} > K^+ > Na^+ > Mg^{2+}$ in 2012 and $NH_4^+ > NO_3^- >> SO_4^{2-} >> Ca^{2+} > K^+ \approx Cl^- > Na^+ > Mg^{2+}$ in 2014. In both campaigns, therefore, NH_4^+ and NO_3^- represent the great majority of water-soluble ions. These ions are widely recognised as secondary pollutants deriving from NH_3 and NO_2, which are commonly emitted by farming activities and vehicular traffic, respectively [1,38]. The Pearson's correlation matrix calculated for water-soluble ions (Table S8) suggests that the two predominant salts in 2012 samples are NH_4NO_3 (0.985) and $(NH_4)HSO_4/(NH_4)_2SO_4$ (0.551). On the other hand, in 2014 samples KCl (0.842), $Mg(NO_3)_2$ (0.640) and $Ca(NO_3)_2$ (0.552) were also present, besides NH_4NO_3 (0.942) and $(NH_4)HSO_4/(NH_4)_2SO_4$ (0.547) [38]. The remarkable presence of NH_4NO_3 in the samples collected in both campaigns is likely due to the distance of Turin from the sea and, therefore, to the presence of only small quantities of NaCl in the aerosol of the city. This salt, indeed, is the main sink of NH_4NO_3 in the aerosol of maritime cities [39]. The mass ratio of NO_3^-/SO_4^{2-}, commonly used as an indicator of the relative contribution of mobile and stationary sources in the atmosphere [40,41], is almost always higher than one, suggesting that the mobile source emissions were predominant. This represents a further confirmation of the important role that the vehicular traffic plays in determining the composition of the Turin metropolitan area atmosphere.

Considering the limit values reported in the European Directive 2004/107/EC and 2008/50/EC (As, Cd, Ni, Pb, and PM_{10} limit concentrations of 6 ng/m^3, 5 ng/m^3, 20 ng/m^3, 0.5 µg/m^3, and 50 µg/m^3, respectively), no exceedances were registered for As and Pb in the investigated periods. One exceedance was registered for Cd in 2014. However, this is an isolated case, since overall the concentration of Cd in 2014 samples was not higher than in 2012. Indeed, the median concentrations found for this element in 2012 and 2014 samples are 320 and 291 pg/m^3, respectively. Regarding Ni, one exceedance was registered in 2012 and four exceedances in 2014. In this case, this outcome is accompanied by an overall increase in the Ni concentration, since the median concentrations found for this element in 2012 and 2014 samples are 4.06 and 7.67 ng/m^3, respectively. Conversely, the exceedances of the limit value provided for the PM_{10} concentration were more frequent in 2012, as 24 and 8 exceedances were registered in 2012 and 2014, respectively. Taking into account the average composition of the PM_{10} samples shown in Figure 2, this difference seems attributable to the undetermined portion of PM. This fact can be explained considering that the period October–December 2012 was characterized by a lower number of atmospheric precipitation days with respect to the same period in 2014 (21 and 35, respectively) and by a lower amount of atmospheric precipitation (181 and 318 mm, respectively). Moreover, lower temperatures (median: 7.4 and 10 °C, respectively) and slightly lower maximum mixing heights (725 and 748 m, respectively) were also registered, i.e., atmospheric conditions which favor the deposition of the fine fraction of PM, generally richer in organic and elemental carbon.

In order to accomplish a first subdivision of elements according to their primary source (i.e., crustal or anthropogenic), crustal enrichment factors (CEFs) were calculated as explained in [42]. The upper crust composition reported by Wedepohl [43] and Al as a reference element were used for the calculations. Figure 3 shows the box plot of CEFs separately calculated for the two sampling campaigns.

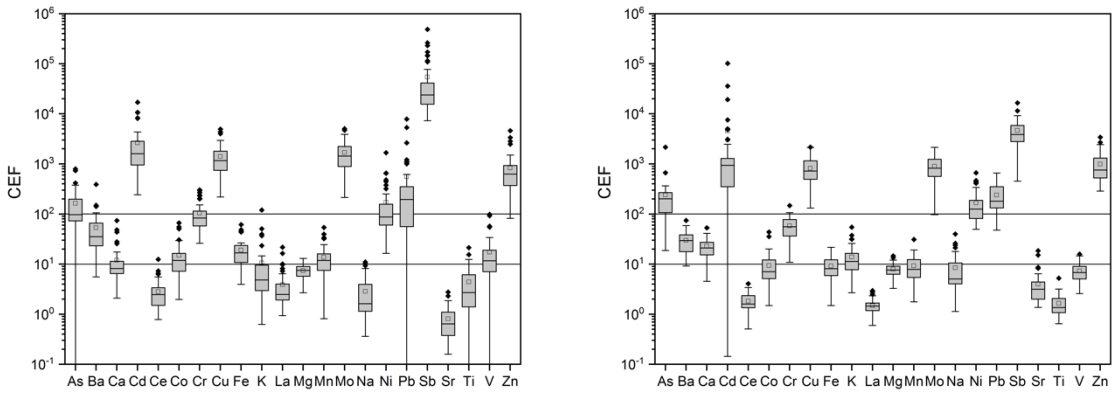

Figure 3. Box plots of crustal enrichment factors (CEFs) calculated with respect to the upper crust composition reported by Wedepohl [43] for (**a**) 2012 samples; (**b**) 2014 samples.

From the calculated CEFs (Table S9) it emerged that the origin of Ce, La, Mg, Sr, and Ti is mostly geogenic, As, Cd, Cr, Cu, Mo, Ni, Pb, Sb, and Zn seem to mainly derive from anthropogenic sources and Ba, Ca, Co, Fe, K, Mn, and V seem to have a mixed crustal-anthropogenic origin. No marked differences can be seen among the two campaigns in the attribution of elements to their primary source. However, the Mann–Whitney test proved that the CEFs of As, Ca, K, Na, Ni, Sr, and Zn significantly rose from 2012 to 2014, indicating an increase of the non-geogenic portion of these analytes in PM.

A comprehensive PCA including data from the two sampling campaigns (2012 and 2014) was executed. Besides the concentrations of the inorganic components of the PM_{10} samples, both the concentrations of $PM_{2.5}$, PM_{10}, NO, and NO_2 and the meteorological parameters (i.e., average and maximum wind speed, average and maximum mixing height, and average temperature) were included in the dataset. The first PC (32.65% of variance, Supplementary Figure S1) represents the general

presence of inorganic pollutants in the Beinasco atmosphere, since NO, NO_2, $PM_{2.5}$, PM_{10}, and all the species determined in the PM_{10} samples present positive loadings on this PC. The average and maximum wind speed present negative loadings on PC1, indicating that they are generally anticorrelated with the total air pollution load. The position of samples along this PC seems completely unrelated with the sampling campaign or the sampling month. Interestingly, most Saturday and the great majority of Sunday samples present negative scores on PC1 and, therefore, were characterized by a higher urban air quality. This fact, which is less evident in the pre-Christmas days, is likely a consequence of the reduced vehicular traffic during non-working days.

Score and loading plots obtained for PC2 vs. PC3 (16.40% and 9.11% of variance, respectively) are shown in Figure 4. PC2 allows an almost perfect separation of the samples collected in 2012 and 2014, as almost all of them have negative and positive scores on this PC, respectively. The variables having the highest negative loadings on PC2 are NO and NO_2, while As, Ca, K, Na, Sr, and Zn have the highest positive loadings. Therefore, the latter group of analytes is characterized by higher concentrations in 2014 than in 2012 samples. The average temperature presents negative loadings on PC2 and positive loadings on PC3. Indeed, it is possible to see that the last three months of 2014 were generally warmer than the same months of 2012 and that, each year, the temperature lowered as the season progressed. As expected, the average and maximum mixing height are strongly correlated with the average temperature. Moreover, the coldest period of 2012 is characterized by the highest concentration of K^+, a typical marker of biomass burning [40,44–46], probably due to a greater use of stoves and fireplaces for domestic heating.

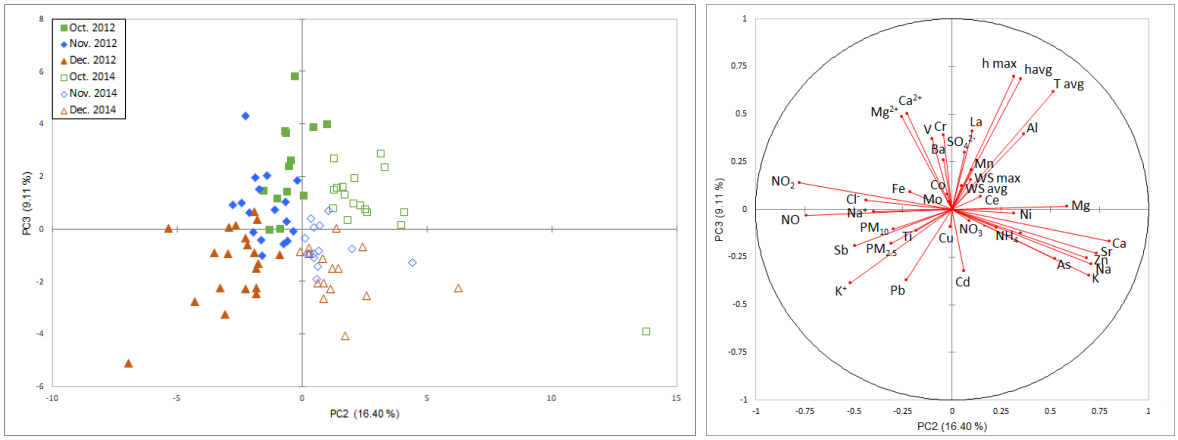

(**a**) (**b**)

Figure 4. Principal component analysis (PC2 vs. PC3) for 2012 and 2014 samples: (**a**) score plot; (**b**) loading plot. WS avg = average wind speed; WS max = maximum wind speed; h avg = average mixing height; h max = maximum mixing height; T avg = average temperature.

Mann–Whitney test was performed for checking if the analyte concentrations determined in 2012 and 2014 samples were significantly different. In addition to the elements causing a good differentiation of the two campaigns in PCA (i.e., As, Ca, K, Na, Sr, and Zn), the concentration of Al, Ba, Ni, and Pb also resulted significantly higher in 2014 than in 2012 samples. Among these, as reported above, the CEFs significantly rose for As, Ca, K, Na, Ni, Sr, and Zn, suggesting that the concentration increase of these elements was due to non-geogenic sources. For trying to give a quantitative estimate of this variation, the maximum and average increment (expressed as percentage) from 2014 to 2012 was calculated. Moreover, the exceedance frequency in 2014 was calculated as percentage considering the number of samples with higher concentrations in 2014 than the 2012 maximum value and the total number of 2014 samples. In the investigated period, exceedance frequencies of 15%, 9%, 28%, 24%, 9%, 80%, and 35% were registered for As, Ca, K, Na, Ni, Sr, and Zn, respectively. The concentration

increment, for the exceedance days, was on average 21%, 25%, 10%, 26%, 31%, 7%, and 15%, and maximum 63%, 77%, 80%, 85%, 65%, 96%, and 77% for As, Ca, K, Na, Ni, Sr, and Zn, respectively.

Figure 4b shows that a good correlation exists among all these elements except Ni and, therefore, it is likely that a common source arose for As, Ca, K, Na, Sr, and Zn in 2014. Direct incinerator emissions are conceivable sources for As, K, Na, and Zn: Zn is the most common elemental marker of incinerator emissions [13,14,47–50], but As is also reported to be emitted by incinerator plants [18,47,49,51]; the behavior of Na may be explained considering that $NaHCO_3$ is used at the Turin incinerator plant for the abatement of acids from vapor emissions [21], while K is a common marker of biomass burning events [14]. Considering the position of K^+ and K in the loading plot, in particular with respect to Zn and T avg, it is possible to hypothesize that the water-soluble form of K is the most strongly related to domestic heating, while its total content might include a contribution from a different source. However, Zn is also a common marker of tyre wear [52,53], and its correlation with Ca, a typical crustal element, might also indicate road dust resuspension phenomena. It should also be noted that the periodic sampling of the direct incinerator emissions made by ARPA Piemonte in October and November 2014 showed Zn concentration lower than 20 ng/m^3 for each incinerator line [21].

For trying to evaluate if the increment of the concentration of these elements might have been caused by the incinerator emissions, pollution roses were realized with the Openair R-package for 2014 samples, combining the analyte concentration with the prevailing wind direction. It is important to note, though, that in 2014 the wind very rarely blew from the direction of the incinerator during the investigated months. However, the height of the incinerator chimney is 120 m and, therefore, the area most strongly affected by the incinerator emissions is not necessarily determined by the wind direction at the ground level. Moreover, considering that the area was generally characterized by "calm" or "light air" conditions (Beaufort wind force scale, wind speed <1.5 m/s), significant incinerator emissions would have been detected, yet they would have been unrelated to the wind direction. By looking at the pollution roses reported in Figure 5, it is evident that the highest concentrations of all the elements, except Ni, were registered when the wind prevalently blew from south southwest or southwest. Taking into account that the incinerator is located northwest of the monitoring station (Figure 1), it seems that the concentration increment was not directly caused by the plant emissions. However, considering the position of the monitoring station, the most probable source of these elements is the highway located southwest of the incinerator. Hence, it is likely that the concentration increment was caused by the increased frequency of heavy vehicles travelling the highway, because of the trucks carrying the waste to the incinerator. Nevertheless, a direct contribution deriving from the incinerator emissions cannot be excluded. The concentration of Ni was the highest when the wind prevalently blew from east northeast, i.e., from the centre of Turin. A contribution from the city vehicular traffic is conceivable for this analyte.

The pollution roses realized for the other analytes are reported in Supplementary Figure S2. The concentrations of all the analytes except Sb were particularly high when the wind prevalently blew from south southwest. Moreover, a source of Ca^{2+}, Cl^-, Cr, Fe, K^+, Mg^{2+}, Mo, Na^+, Sb, SO_4^{2-}, Ti, and V was present southeast, a source of Cl^-, Fe, Mg^{2+}, Na^+, NO_2, and Ti was present northeast.

In order to compare the composition of the PM_{10} samples collected in the investigated area with the composition of samples collected in other parts of the city, Table 1 reports the descriptive statistics (average concentration, the 5th and 95th percentile) of this work results and the concentration ranges found by Padoan et al. [54] in other two sampling sites in Turin. Although the concentration increase discussed above (e.g., for As, Ca, K, Ni, Sr, and Zn) is evident, all the mean analyte concentrations found in this work for both 2012 and 2014 campaigns are within the concentration ranges taken for comparison. This result confirms that the composition of the PM_{10} samples collected in the vicinity of the incinerator and in other parts of the city is similar. This can be explained considering the great role that vehicular emissions play in determining the Turin air quality.

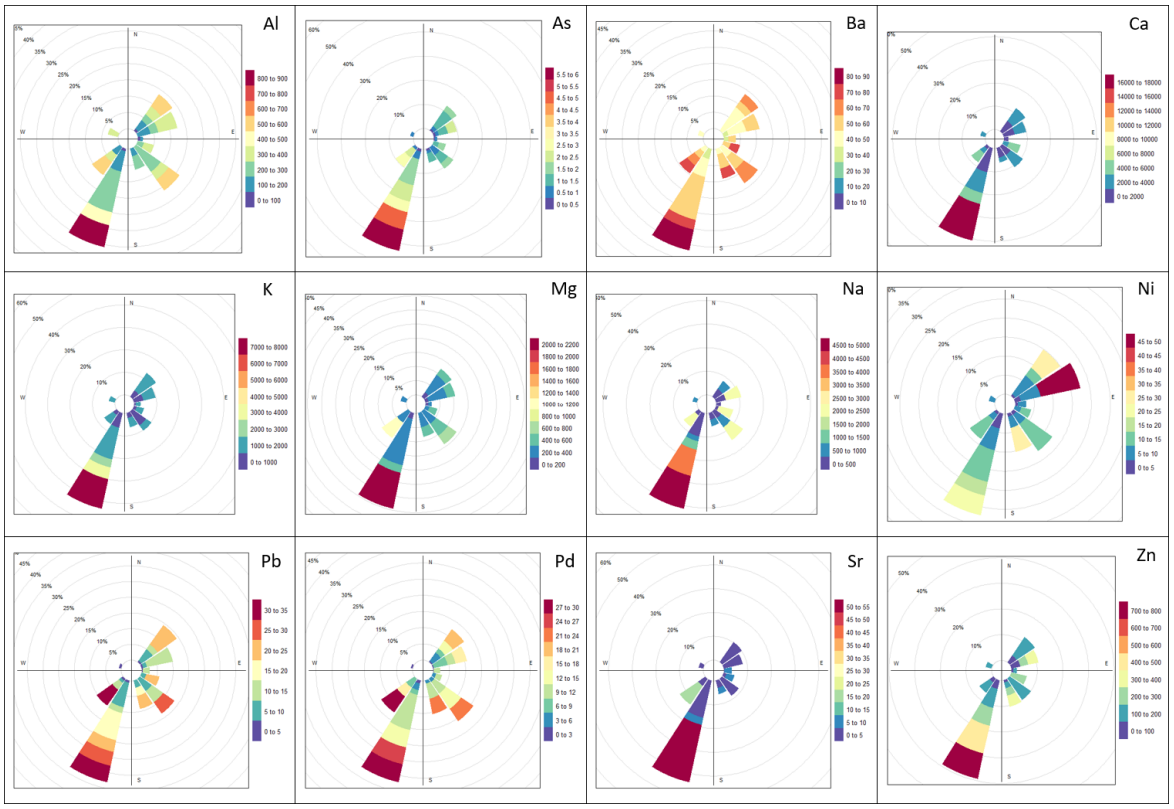

Figure 5. Pollution roses for 2014 samples, showing a combination of the analyte concentration (ng/m^3) and the prevailing wind direction.

Table 1. Descriptive statistics of the inorganic composition of the PM_{10} collected in 2012 and 2014. For comparison, the concentration ranges found by Padoan et al. [36] in other two sampling sites are also reported. All the concentrations are expressed in ng/m^3.

	2012		2014		2011 TO1 [36]	2011 TO2 [36]
	Mean	5th–95th perc.	Mean	5th–95th perc.	Range	Range
Al	170	33–470	250	98–530	18–430	12–1100
As	0.48	0.059–1.7	1.1	0.26–2.9	0.18–1.5	0.19–4.7
Ba	48	19–150	52	40–78	12–77	7.4–100
Ca	580	140–1200	1700	840–5000	19–1500	270–2700
Cd	0.32	0.12–0.83	0.29	0.020–2.7	0.19–1.1	0.32–5.5
Ce	0.33	0.076–0.66	0.34	0.16–0.65	0–0.88	2.1–6.0
Co	0.32	0.036–1.1	0.31	0.082–0.64	0.06–1.7	0.09–1.5
Cr	6.4	2.4–12	5.2	2.3–12	1.9–14	2.6–34
Cu	40	7.8–79	27	11–77	5.0–52	13–180
Fe	1200	260–2200	720	230–1700	270–3200	430–6800
K	360	61–1100	860	330–2100	79–1300	130–910
La	0.19	0.076–0.34	0.12	0.060–0.34	<0.007	2.1–4.0
Mg	190	44–460	290	170–600	19–740	53–1600
Mn	14	2.6–27	12	3.3–30	3.6–37	6.2–96
Mo	3.4	1.6–7.3	3.4	1.1–7.3	0.83–16	1.3–14
Ni	4.1	0.58–9.3	7.7	2.9–25.3	0–16	2.2–15
Pb	8.5	0–26	10	3.2–25	3.8–45	0–40
Sb	17	5.0–56	3.9	0.83–8.8	1.9–48	2.6–28
Sr	0.35	0.12–1.5	3.1	1.1–7.1	0.04–4.4	0.44–11
Ti	19	1.9–51	16	5.0–34	2.3–54	5.7–65
V	1.3	0.20–3.1	1.2	0.34–2.2	1.1–5.7	0.73–5.7
Zn	68	19–160	130	45–390	20–160	15–230

4. Conclusions

In this study, the evolution of the inorganic composition of PM_{10} collected in the vicinity of the Turin incinerator before and after its commissioning was assessed. The purpose was to identify the PM sources present in the area, and to evaluate if the operation of the incinerator caused an increase of the concentration of some species. A total of 50 samples collected from October to December 2012 and 46 samples collected from October to December 2014 were analyzed.

The metal concentration limits provided by the European Directives were seldom exceeded, while the exceedances of the limit value provided for the PM_{10} concentration were much more frequent, especially in 2012. The concentration of PM_{10} and, therefore, of its inorganic constituents proved higher in lower wind speed conditions and on working days. In addition, a peak of the concentration of K^+ was registered during the coldest days of 2012, probably due to a greater use of stoves and fireplaces for domestic heating.

Significant differences were registered between the composition of samples collected in 2012 and 2014, as the latter year was characterized by higher concentrations of the anthropogenic portion of As, Ca, K, Na, Ni, Sr, and Zn. The concentrations of Zn, i.e., the most common marker of incinerator emissions, exceeded the maximum 2012 concentration in 35% of 2014 samples. The concentration increment was of 15% on average, with a peak of 77%. However, considering the position of the incinerator and of the monitoring station, it seems that this increment was not directly caused by the plant emissions, yet by the highway vehicular traffic, which might have increased due to the travelling of trucks carrying wastes to the incinerator. Nevertheless, a direct contribution deriving from the incinerator emissions cannot be excluded.

Supplementary Materials: The following are available online at http://www.mdpi.com/2073-4433/11/4/400/s1, Table S1: Model and features of the analytical instruments used for the analysis, Table S2: Analytical parameters optimized for each analyte, and experimental detection limits (DL), Table S3: Meteorological data, PM_{10} and $PM_{2.5}$ mass concentrations ($\mu g/m^3$), and NO and NO_2 atmospheric concentrations ($\mu g/m^3$) used for the choice of the samples to analyze (a) samples collected in 2012; (b) samples collected in 2014, Table S4: Water-soluble ionic components and major element concentrations in 2012 samples. All the results are expressed in ng/m^3, except NH_4^+, NO_3^-, and SO_4^{2-} which are expressed in $\mu g/m^3$, Table S5: Minor and trace element concentrations in 2012 samples. All the results are expressed in ng/m^3, except As, Cd, Ce, Co, and La which are expressed in pg/m^3, Table S6: Water-soluble ionic components and major element concentrations in 2014 samples. All the results are expressed in ng/m^3, except NH_4^+, NO_3^-, and SO_4^{2-} which are expressed in $\mu g/m^3$, Table S7: Minor and trace element concentrations in 2014 samples. All the results are expressed in ng/m^3, except As, Cd, Ce, Co, and La which are expressed in pg/m^3, Table S8: Pearson's correlation matrix for water-soluble ions in (a) 2012 samples; (b) 2014 samples, Table S9: Crustal enrichment factors calculated with respect to the upper crust composition reported by Wedepohl [43] for (a) 2012 samples; (b) 2014 samples, Figure S1: Principal component analysis (PC1 vs. PC2) for 2012 and 2014 samples: (a) score plot; (b) loading plot, Figure S2: Pollution roses for 2014 samples, showing a combination of the analyte concentration (ng/m^3) and the prevailing wind direction.

Author Contributions: Conceptualization, M.M.; Formal Analysis, E.C.; Investigation, E.C.; Methodology, S.B. (Stefano Bande); Resources, M.M., O.A., S.B.(Sandro Buoso), S.B. (Stefano Bande), M.S. and A.G.; Data Curation, S.B.(Stefano Bande) and M.S.; Writing—Original Draft Preparation, E.C.; Writing—Review and Editing, M.M., O.A., P.I. and A.G.; Visualization, E.C.; Supervision, M.M.; Project Administration, M.M.; Funding Acquisition, M.M., O.A. and A.G. All authors have read and agreed to the published version of the manuscript.

Funding: This research received no external funding.

Acknowledgments: The authors thank Ylenia Accossato and Edoardo Rossi for carrying out the chemical analysis of samples.

Conflicts of Interest: The authors declare no conflict of interest.

References

1. Finlayson-Pitts, B.J.; Pitts, J.N.J. *Chemistry of the Upper and Lower Atmosphere*; Academic Press: Cambridge, MA, USA, 1999.
2. Wallace, J.M.; Hobbs, P.V. *Atmospheric Science*; Elsevier Academic Press: Amsterdam, The Netherlands, 2006.

3. Pope, C.A.I.; Burnett, R.T.; Thun, M.J.; Calle, E.E.; Krewski, D.; Ito, K.; Thurston, G. Lung cancer, cardiopulmonary mortality, and long-term exposure to fine particulate air pollution. *J. Am. Med Assoc.* **2002**, *287*, 1132–1141. [CrossRef]
4. Costa, D.L.; Dreger, K.L. Bioavailable transition metals in particulate matter mediate cardiopulmonary injury in healthy and compromised animal models. *Environ. Earth Perspect.* **1997**, *105*, 1053.
5. Mukhtar, A.; Limbeck, A. Recent developments in assessment of bio-accessible trace metal fractions in airborne particulate matter: A review. *Anal. Chim. Acta* **2013**, *774*, 11–25. [CrossRef] [PubMed]
6. Pelfrene, A.; Cave, M.R.; Wragg, J.; Douay, F. In Vitro Investigations of Human Bioaccessibility from Reference Materials Using Simulated Lung Fluids. *Int. J. Environ. Res. Pub. Health* **2017**, *14*, 112. [CrossRef] [PubMed]
7. Asgharian, B.; Hofmann, W.; Bergmann, R. Particle Deposition in a Multiple-Path Model of the Human Lung. *Aerosol Sci. Technol.* **2001**, *34*, 332–339. [CrossRef]
8. Oberdörster, G.; Oberdörster, E.; Oberdörster, J. Nanotoxicology: An Emerging Discipline Evolving from Studies of Ultrafine Particles. *Environ. Health Perspect.* **2005**, *113*, 823–839. [CrossRef]
9. Cassee, F.R.; Héroux, M.E.; Gerlofs-Nijland, M.E.; Kelly, F.J. Particulate matter beyond mass: Recent health evidence on the role of fractions, chemical consttuents ans sources of emission. *Inhal. Toxicol.* **2013**, *25*, 802–812. [CrossRef]
10. Grigoratos, T.; Martini, G. Brake wear particle emissions: A review. *Environ. Sci. Pollut. Res.* **2015**, *22*, 2491–2504. [CrossRef]
11. Thorpe, A.; Harrison, R.M. Sources and properties of non-exhaust particulate matter from road traffic: A review. *Sci. Total Environ.* **2008**, *400*, 270–282. [CrossRef]
12. Amato, F. *Non-Exhaust Emissions*; Elsevier: Amsterdam, The Netherlandas, 2018.
13. Li, Y.; Zhang, H.; Shao, L.; Zhou, X.; He, P. Impact of municipal solid waste incineration on heavy metals in the surrounding soils by multivariate analysis and lead isotope analysis. *J. Environ. Sci.* **2019**, *82*, 47–56. [CrossRef]
14. Lucarelli, F.; Barrera, V.; Becagli, S.; Chiari, M.; Giannoni, M.; Nava, S.; Traversi, R.; Calzolai, G. Combined use of daily and hourly data sets for the source apportionment of particulate matter near a waste incinerator plant. *Environ. Pollut.* **2019**, *247*, 802–811. [CrossRef]
15. Panepinto, D.; Zanetti, M.C. Municipal solid waste incineration plant: A multi-step approach to the evaluation of an energy-recovery configuration. *Waste Manag.* **2018**, *73*, 332–341. [CrossRef]
16. Caviglia, C.; Confalonieri, G.; Corazzari, I.; Destefanis, E.; Mandrone, G.; Pastero, L.; Boero, R.; Pavese, A. Effects of particle size on properties and thermal inertization of bottom ashes (MSW of Turin's incinerator). *Waste Manag.* **2019**, *84*, 340–354. [CrossRef] [PubMed]
17. Panepinto, D.; Genon, G. Environmental evaluation of the electric and cogenerative configurations for the energy recovery of the Turin municipal solid waste incineration plant. *Waste Manag. Res.* **2014**, *32*, 670–680. [CrossRef]
18. Maître, A.; Collot-Fertey, D.; Anzivino, L.; Marques, M.; Hours, M.; Stoklov, M. Municipal waste incinerators: Air and biological monitoring of workers for exposure to particles, metals, and organic compounds. *Occup. Environ. Med.* **2003**, *60*, 563–569. [CrossRef] [PubMed]
19. Meneses, M.; Schuhmacher, M.; Domingo, J.L. Health risk assessment of emissions of dioxins and furans from a municipal waste incinerator: Comparison with other emission sources. *Environ. Int.* **2004**, *30*, 481–489. [CrossRef] [PubMed]
20. Schuhmacher, M.; Domingo, J.L. Long-term study of environmental levels of dioxins and furans in the vicinity of a municipal solid waste incinerator. *Environ. Int.* **2006**, *32*, 397–404. [CrossRef]
21. TRM S.p.A.—Trattamento Rifiuti Metropolitani. Available online: http://trm.to.it/en/ (accessed on 2 March 2020).
22. Desiato, F.; Finardi, S.; Brusasca, G.; Morselli, M.G. TRANSALP 1989 Experimental campaign—Part I: Simulation of 3-D flow with diagnostic wind field models. *Atmos. Environ.* **1998**, *32*, 1141–1156. [CrossRef]
23. Finardi, S.; De Maria, R.; D'Allura, A.; Cascone, C.; Calori, G.; Lollobrigida, F. A deterministic air quality forecasting system for Torino urban area, Italy. *Environ. Model. Softw.* **2008**, *23*, 344–355. [CrossRef]
24. Cameletti, M.; Ignaccolo, R.; Bande, S. Comparing spatio-temporal models for particulate matter in Piemonte. *Environmetrics* **2011**, *22*, 985–996. [CrossRef]
25. Bande, S.; D'Allura, A.; Finardi, S.; Giorcelli, M.; Muraro, M. Meteorological modelling influence on regional and ur-ban air pollution predictability. *Croat. Meteorol. J.* **2008**, *43*, 613–617.

26. Gariazzo, C.; Silibello, C.; Finardi, S.; Radice, P.; Piersanti, A.; Calori, G.; Cecinato, A.; Perrino, C.; Nussio, F.; Cagnoli, M.; et al. A gas/aerosol air pollutants study over the urban area of Rome using a comprehensive chemical transport model. *Atmos. Environ.* **2007**, *41*, 7286–7303. [CrossRef]
27. Finardi, S.; Baklanov, A.; Clappier, A.; Fay, B.; Joffre, S.; Karppinen, A.; Ødegård, V.; Slørdal, L.H.; Sofiev, M.; Sokhi, R.S.; et al. *FUMAPEX Report: Improved Interfaces and Meteorological Pre-processors for Urban Air Pollution Models*; Milan, Italy, 2005.
28. Calori, G.; Clemente, M.; De Maria, R.; Finardi, S.; Lollobrigida, F.; Tinarelli, G. Air quality integrated modelling in Turin urban area. *Environ. Model. Softw.* **2006**, *21*, 468–476. [CrossRef]
29. Maul, P.R.; Barber, F.R.; Martin, A. Some observations of the meso-scale transport of sulphur compunds in the rural East Midlands. *Atmos. Environ.* **1980**, *14*, 339–354. [CrossRef]
30. Nieuwstadt, F.T.M. The steady-state height and resistance laws of the nocturnal boundary layer: Theory compared with Cabauw observations. *Bound. Layer Meteorol.* **1981**, *2*, 3–17. [CrossRef]
31. Venkatram, A. Estimating the Monin-Obukhov length in the stable boundary layer for dispersion calculations. *Bound. Layer Meteorol.* **1980**, *19*, 481–485. [CrossRef]
32. Einax, W.; Zwanziger, H.W.; Gei, S. *Chemometrics in Environmental Analysis*; Wiley-VHC: Weinhem, Germany, 1997.
33. Massart, D.L.; Vandenginste, B.G.M.; Buydens, L.M.C.; De Jono, S.; Leqi, P.J.; Smeyers-Verbeke, J. *Handbook of Chemometrics and Qualimetrics, Parts A and B*; Elsevier: Amsterdam, The Netherlands, 1997.
34. Mann, H.B.; Whitney, D.R. On a test of whether one of two random variables is stochastically larger than the other. *Ann. Math. Stat.* **1947**, *18*, 50–60. [CrossRef]
35. Ruxton, G.D.; Beauchamp, G. Some suggestions about appropriate use of the Kruskal–Wallis test. *Anim. Behav.* **2008**, *76*, 1083–1087. [CrossRef]
36. Sheppard, P.R.; Helsel, D.R.; Speakman, R.J.; Ridenour, G.; Witten, M.L. Additional analysis of dendrochemical data of Fallon, Nevada. *Chem. Biol. Interact.* **2012**, *196*, 96–101. [CrossRef]
37. Farnham, I.M.; Singh, A.K.; Stetzenbach, K.J.; Johannesson, K.H. Treatment of nondetects in multivariate analysis of groundwater geochemistry data. *Chemom. Intell. Lab.* **2002**, *60*, 265–281. [CrossRef]
38. Fan, J.; Yue, X.; Jing, Y.; Chen, Q.; Wang, S. Online monitoring of water-soluble ionic composition of PM10 during early summer over Lanzhou City. *J. Environ. Sci.* **2014**, *26*, 353–361. [CrossRef]
39. Ochsenkühn, K.M.; Lyberopoulou, T.; Koumarianou, G.; Ochsenkühn-Petropoulou, M. Ion chromatographic and spectrometric determination of water-soluble compounds in airborne particulates, and their correlations in an industrial area in Attica, Greece. *Microchim. Acta* **2007**, *160*, 485–492. [CrossRef]
40. Zhou, J.; Xing, Z.; Deng, J.; Du, K. Characterizing and sourcing ambient PM2.5 over key emission regions in China I: Water-soluble ions and carbonaceous fractions. *Atmos. Environ.* **2016**, *135*, 20–30. [CrossRef]
41. Khoder, M.I.; Hassan, S.K. Weekday/weekend differences in ambient aerosol level and chemical characteristics of water-soluble components in the city centre. *Atmos. Environ.* **2008**, *42*, 7483–7493. [CrossRef]
42. Conca, E.; Abollino, O.; Giacomino, A.; Buoso, S.; Traversi, R.; Becagli, S.; Grotti, M.; Malandrino, M. Source identification and temporal evolution of trace elements in PM10 collected near to Ny-Ålesund (Norwegian Arctic). *Atmos. Environ.* **2019**, *203*, 153–165. [CrossRef]
43. Wedepohl, K.H. The composition of the continental crust. *Geochim. Cosmochim. Acta* **1995**, *59*, 1217–1232. [CrossRef]
44. Brehmer, C.; Lai, A.; Clark, S.; Shan, M.; Ni, K.; Ezzati, M.; Yang, X.; Baumgartner, J.; Schauer, J.J.; Carter, E. The Oxidative Potential of Personal and Household PM2.5 in a Rural Setting in Southwestern China. *Environ. Sci. Technol.* **2019**, *53*, 2788–2798. [CrossRef]
45. Tao, J.; Zhang, L.; Engling, G.; Zhang, R.; Yang, Y.; Cao, J.; Zhu, C.; Wang, Q.; Luo, L. Chemical composition of PM2.5 in an urban environment in Chengdu, China: Importance of springtime dust storms and biomass burning. *Atmos. Res.* **2013**, *122*, 270–283. [CrossRef]
46. Benetello, F.; Squizzato, S.; Hofer, A.; Masiol, M.; Khan, M.B.; Piazzalunga, A.; Fermo, P.; Formenton, G.M.; Rampazzo, G.; Pavoni, B. Estimation of local and external contributions of biomass burning to PM2.5 in an industrial zone included in a large urban settlement. *Environ. Sci. Pollut. Res.* **2017**, *24*, 2100–2115. [CrossRef]
47. Pancras, J.P.; Ondov, J.M.; Poor, N.; Landis, M.S.; Stevens, R.K. Identification of sources and estimation of emission profiles from highly time-resolved pollutant measurements in Tampa, FL. *Atmos. Environ.* **2006**, *40*, 467–481. [CrossRef]

48. Pancras, J.P.; Ondov, J.M.; Zeisler, R. Multi-element electrothermal AAS determination of 11 marker elements in fine ambient aerosol slurry samples collected with SEAS-II. *Anal. Chim. Acta* **2005**, *538*, 303–312. [CrossRef]
49. Sakata, M.; Kurata, M.; Tanaka, N. Estimating contribution from municipal solid waste incineration to trace metal concentrations in Japanese urban atmosphere using lead as a marker element. *Geochem. J.* **2000**, *34*, 23–32. [CrossRef]
50. Suarez, A.E.; Ondov, J.M. Ambient aerosol concentrations of elements resolved by size and by source: Contributions of some cytokine-active metals from coal- and oil-fired power plants. *Energy Fuels* **2002**, *16*, 562–568. [CrossRef]
51. Font, A.; De Hoogh, K.; Leal-Sanchez, M.; Ashworth, D.C.; Brown, R.J.C.; Hansell, A.L.; Fuller, G.W. Using metal ratios to detect emissions from municipal waste incinerators in ambient air pollution data. *Atmos. Environ.* **2015**, *113*, 177–186. [CrossRef]
52. Hwang, H.M.; Fiala, M.J.; Park, D.; Wade, T.L. Review of pollutants in urban road dust and stormwater runoff: Part 1. Heavy metals released from vehicles. *Int. J. Urban Sci.* **2016**, *20*, 334–360. [CrossRef]
53. Mummullage, S.; Egodawatta, P.; Ayoko, G.A.; Goonetilleke, A. Use of physicochemical signatures to assess the sources of metals in urban road dust. *Sci. Total Environ.* **2016**, *541*, 1303–1309. [CrossRef] [PubMed]
54. Padoan, E.; Malandrino, M.; Giacomino, A.; Grosa, M.M.; Lollobrigida, F.; Martini, S.; Abollino, O. Spatial distribution and potential sources of trace elements in PM10 monitored in urban and rural sites of Piedmont Region. *Chemosphere* **2016**, *145*, 495–507. [CrossRef] [PubMed]